Thermal proteome profiling identifies glucose binding proteins involved in metabolic disease

Ian D. Ferguson[1,2,5], Lindsey M. Meservey[1,3,5], Vivian Tien[1], Weili Miao[1], Vanessa Lopez-Pajares[1], Douglas F. Porter[1], Paul A. Khavari[1,4,*]

1. Program in Epithelial Biology, Stanford University School of Medicine, Stanford, CA, USA
2. Program in Cancer Biology, Stanford University, Stanford, CA, USA
3. Program in Biology, Stanford University, Stanford, CA, USA
4. Veterans Affairs Palo Alto Healthcare System, Palo Alto, CA, USA
5. Equal contribution

*Correspondence: khavari@stanford.edu

Abstract

Recent work has shown that glucose can modulate protein multimerization and function independent of metabolism through direct protein binding. We sought to build on this work by adapting thermal proteome profiling screens to uncover novel glucose binders involved in metabolism. We found that TSC22D4, an intrinsically-disordered, leucine-zipper protein previously linked to insulin resistance and liver fat accumulation, exhibits altered thermal stability in the presence of glucose. Furthermore, glucose decreased TSC22D4 DNA binding and altered TSC22D4 protein-protein association. Employing UV-crosslinking mass spectrometry, we found glucose binds near the C-terminal leucine zipper domain. Mutating isoleucine 322 to tryptophan (I322W) abolishes glucose binding. Crosslinking-MS and chemo-proteomic experiments suggest that glucose increases accessibility of the leucine zipper region, resulting in intra-protein contacts between C-terminal zipper domain and N-terminal intrinsically-disordered domain. TSC22D4 is essential for adipogenesis in the 3T3-L1 model system, and glucose can increase nuclear localization of TSC22D4 and remodel its protein-protein interactions. Finally, we further extend this work by validating site-specific glucose binding for another PISA target with genetic linkage to metabolic disease.

Introduction

Recent efforts have illustrated the capacity of protein-metabolite interactions to drive protein function (Liu et al. 2023). For example, glucose binding to proteins including IRF6, DDX21, DDX50, and NSUN2 modulate transcription, RNA-binding, and cellular localization (Lopez-Pajares et al. 2025; Miao et al. 2023; Chen et al. 2023; Miao et al. 2024). In a seminal study, glucose gradients formed during stratified epithelial differentiation lead to induction of binding events in key drivers of differentiation. (Lopez-Pajares et al. 2025; Miao et al. 2023). Specifically, glucose binding leads to dimerization and genome targeting of IRF6, a pioneer transcription factor in keratinocyte differentiation, which drives induction of differentiation related genes (Lopez-Pajares et al. 2025). Glucose accumulation and binding leads to de-dimerization and re-localization of DDX21, which alters RNA-splicing to drive differentiation (Miao et al. 2023).

Importantly, these glucose binding proteins were identified by affinity purification mass spectrometry strategies using dextran column or biotin-glucose probes, which both require modified glucose derivatives. Another rapidly developing approach to study small protein-ligand interactions is thermal proteome profiling (TPP), which measures binding-induced changes in thermal solubility with unmodified metabolites (Gaetani et al. 2019; Franken et al. 2015; Liu et al. 2023). In this work, we apply thermal proteome profiling methods to identify new glucose binding proteins and characterize the effect of glucose binding on protein function for two new glucose binding, TSC22D4 and IGF2BP2, which have published genetic linkage to fatty liver disease and diabetes, respectively (Demir et al. 2022; Ekim Üstünel et al. 2016; Regué et al. 2021; Regué et al. 2019; Wolff et al. 2022).

Results

Thermal profiling proteomics identifies hexose binding proteins at physiologic concentrations

We first sought to utilize TPP techniques to expand upon existing research identifying glucose binding proteins. Traditionally, TPP has been used to discover high affinity ligand-protein interactions such as small molecule inhibitors (Van Vranken et al. 2024). Recently, TPP of small metabolites was performed in *E. coli* lysate using supraphysiological osmolyte concentrations (Pepelnjak et al. 2024). We hypothesized that TPP at physiological osmolyte concentrations could uncover function hexose-proteins interactions. As a proof of concept, we started with TPP, treating cell lysates with 350 μM glucose and heating along a temperature gradient, collecting soluble fractions, and multiplexing temperatures with TMT-16plex reagents (Fig. S1A). Encouragingly, we saw hexokinases HK1 and HK2 highly solubilized by glucose (Fig 1A-B). We also saw de-solubilization of DDX21, a previously validated glucose binding protein (Miao et al. 2023), as well as ADAR and IGF2BP3, which have been found by prior studies using pulldown MS techniques (Fig. 1A) (Chen et al. 2023; Lopez-Pajares et al. 2025; Miao et al. 2023). Importantly, the majority of proteins did not have a shift in solubility at 350 μM glucose (Fig

S1B). We next moved to proteome-in-solution assays (PISA) (Gaetani et al. 2019), which pool soluble fractions from each temperature, allowing for multiple treatment replicates run in a single TMT experiment (Fig S1A). We validated that glucose-induced solubility of HK1 was visible in a PISA-western, and saw slight solubilization of IRF6, a known glucose binder with a K_d of 144 μM (Lopez-Pajares et al. 2025), illustrating that some glucose binders might be less amenable to thermal shift assays (Fig. S1C-E). Total proteome solubilization was unchanged by glucose, and fold change of glucose induced stabilization of HK1 was similar to that of ATP-induced Actin stabilization (Fig 1G).

Encouraged by these results, we performed PISA assays in cellular lysates treated with glucose and other hexoses looking to find new glucose binding proteins (GBPs). Importantly, in each experiment, HK1 stabilization was seen upon glucose treatment (Fig 1 H-L). In 3T3-L1 lysates treated with glucose, fructose, or galactose, we were able to find previously identified GBP Nsun2 (Chen et al. 2023; Miao et al. 2024), along with putative novel GBPs TSC22D4 and IGF2BP2. Interestingly, glucose induced thermal stability shifts were more correlated with fructose than with galactose, a stereoisomer to glucose (Fig. S1C). We also performed PISA experiments in A431 squamous cell carcinoma lysates using glucose, galactose, and 3-o-methyl-D-glucose (3oMG), a non-metabolizable analog of glucose, finding higher correlation between glucose and 3oMG than glucose and galactose (Fig S1D) and specific shifts in solubility in PIK3 complex subunits and PAK1 (Fig 1I). We next performed PISA experiments in 293T embryonic kidney whole cell lysates and nuclear extracts treated with 1 mM or 5 mM glucose, identifying thermal solubility shifts in proteins including PAK1 and SF3B1 (Fig 1J-L). Among the novel glucose-binding proteins identified by our studies, TSC22D4 and IGF2BP2 stood out in their connection to glucose-related disease (Demir et al. 2022; Ekim Üstünel et al. 2016; Regué et al. 2021; Regué et al. 2019; Wolff et al. 2022). We next validated induced solubility shifts of putative glucose binders using thermal shift westerns. TSC22D4 and IGF2BP3, a homologous family member of IGF2BP2 and expressed in 293t, both had visible solubility decreases when treated with glucose (Fig 1N-O).

TSC22D4 binds glucose at a region around I322

First, we validated TSC22D4 binding to hexose sugars using microscale thermophoresis, finding that TSC22D4 bound fructose with a Kd of 161 μM and glucose with a Kd of 464 μM (Fig 2A). TSC22D4 was also pulled down by B-Glc-Biotin, and binding was decreased by competition with 10 mM glucose (Fig 2B-C). TSC22D4 was originally annotated as a leucine zipper DNA binding protein, and recent work in hepatocytes suggested its DNA binding to the LCN13 promoter regulates insulin response (Ekim Üstünel et al. 2016) (Kester et al. 1999). We found that glucose significantly decreased DNA binding, irrespective of DNA sequence (Fig 2D, Figure S2A). Interestingly, glucose had no significant effect on dimerization using the same MST assay (Fig. 2E), although it did shift TSC22D4 to smaller complexes in a fast-protein liquid chromatography experiment (Fig 2F). In order to identify residues involved in glucose binding, we employed UV-crosslinking mass spectrometry and obtained a high-confidence peptide, IEQAMDLVK, crosslinked to glucose (Fig. 2G, Fig. S2B-C). Mutation I322W ablated glucose binding, while I322P, I322G and triple mutant I322G/E323G/Q324G did not alter glucose binding (Fig. 2 H, Fig S2D-E). We hypothesize that tryptophan mutation at I322 displaces glucose from

a binding pocket in the protein. Importantly, TSC22D4^{I322W} was still able to dimerize, suggesting intact protein biochemical function (Fig. S2F). We next applied a recently developed approach for assessing lysine accessibility using formaldehyde-based chemoproteomics (Tian et al. 2023), and found increased labeling of a C-terminal lysine at position 345 after incubation with glucose (Fig 2J), suggesting increased accessibility of the C-terminal region of the protein. To further understand how glucose modulates TSC22D4 monomeric conformation, we employed BS3 crosslinking on TSC22D4 incubated with glucose, isolating the monomeric band for mass spectrometry (Fig S2G). Glucose incubation induced new long-range contacts between the C-terminus of the protein in the TSC Box to the N-terminus of the protein (Fig 2K), suggesting that glucose might alter TSC box contacts, potentially explaining the decrease in DNA binding, and in agreement with the hypothesis that glucose increases accessibility the C-terminus of TSC22D4.

TSC22D4 is essential for adipogenesis

TSC22D4 has been shown to regulate insulin signaling and AKT activation in hepatocytes (Demir et al. 2022; Ekim Üstünel et al. 2016; Wolff et al. 2022). We wondered if TSC22D4 plays a role in adipocytes, which accumulate glucose during an insulin-dependent differentiation process *in vitro* (Lopez-Pajares et al. 2025; Sadowski et al. 1992)**.** Using shRNAs in the 3T3-L1 adipocyte differentiation model, we found that loss of TSC22D4 impaired differentiation, as indicated by reduced RNA (Fig 3A) and protein expression (Fig 3B, Fig S3A) of adipogenic marker genes and decreased lipid accumulation (Fig 3C, Fig S3B). RNA expression of adipogenesis marker transcripts was rescued by expression of TSC22D4 (Fig S3C-D). Previous work on glucose binding proteins has found that changes in subcellular localization can drive differential function (Miao et al. 2023; Miao et al. 2025), so we performed quantitative IF and found that standard glucose (25 mM) increases nuclear localization of TSC22D4 compared to low glucose (5 mM) (Fig 3D-E). However, in multiple attempts at Cut&Run, we were unable to map genome binding regions for TSC22D4 in 3T3-L1 cells, suggesting that TSC22D4's effect on adipocyte differentiation might not be through its reported function in hepatocytes as a transcriptional repressor (Ekim Üstünel et al. 2016). In support of this, we found that TSC22D4 knockdown did not significantly alter *Lcn13* transcript levels in 3T3-L1 cells (Figure S3E). TSC22D4 has also been reported to scaffold protein-protein interactions (Demir et al. 2022; Amnekar et al. 2024). Therefore, we performed affinity purification (AP)-MS in 3T3-L1 cells in various cell culture media to map the glucose-dependent TSC22D4-interactome. We found that crosslinking in-lysate with BS3 improved pulldown of tagged and endogenous TSC22D4, suggesting crosslinking improved recovery of dimeric TSC22D4 (Fig. 3F). Therefore, we proceeded with BS3-crosslinking for AP-MS, starving 3T3-L1 cells overnight of glucose and treating for 1.5 hours with either glucose, 3oMG, or vehicle. Importantly, we found that the glucose and 3oMG effects on the interactome of TSC22D4 were correlated more strongly than vehicle and 3oMG (Fig. 3G, Fig S3F), suggesting that the majority of 3oMG effects were due to direct binding of glucose and not metabolic and signaling changes in the cell. Shared interactors across all conditions included NRBP2, a previously profiled TSC22D4 interactor (Fig. S3G) (Xiao et al. 2024). TSC22D4 interactions with mitochondrial proteins were increased in glucose conditions, while interactions with Actin/cytoskeleton proteins were enriched in the vehicle treated cells (Fig. 3H-I, Fig. S3H). We hypothesize that glucose-binding induced remodeling of

TSC22D4 protein interactions drives its effect in adipogenesis (Fig. 3J-K). We next wondered if there might be an additional layer of regulation that contributes to TSC22D4 function in insulin-induced adipogenesis. We used a previously generated phosphoproteomic dataset measuring 3T3-L1 response to insulin treatment (Humphrey et al. 2013), and found three phosphorylation sites on TSC22D4—T57, S123, and S271—which were sensitive to insulin treatment (Fig. S3I). Interestingly, mutating the homologous serine to S271 in the human sequence, S279, to alanine ablated TSC22D4-glucose binding, while mutation S279D phosphomimetic preserved glucose binding with a slightly increased affinity (Fig. S3J). One model to explain these results, which can be pursued in future research, is that S279 might form part of the glucose binding pocket in TSC22D4, and that rapid phosphorylation of S279 after insulin stimulation could prime TSC22D4 for glucose binding as levels increase in 3T3-L1s downstream of GLUT4-mediated glucose transport (Hauner et al. 1998).

IGF2BP2 binds glucose at Y40A

We next sought to validate glucose binding to IGF2BP2, another putative target from the PISA screen (Fig 1H,M). IGF2BP2 has been connected to type 2 diabetes by GWAS studies in multiple populations (Diabetes Genetics Initiative of Broad...; Zeggini et al. 2008; Scott et al. 2007), and IGF2BP2 loss improves insulin sensitivity and protects against diet-induced obesity (Regué et al. 2019; Dai et al. 2015). We purified IGF2BP2, performed MST, and found a K_d for glucose of 8.2 μM (Fig 4A). However, in multiple attempts at UV-C mass spec, we were unable to recover a glucose bound peptide. Interestingly, we noticed that IGF2BP3, a homologous family member with 67% identity and 78% similarity to IGF2BP2, was a shared hit in three previous mass spec experiments looking for glucose binding proteins (Fig S4A-B). We hypothesized that UV-C MS on IGF2BP3 might produce a glucose bound peptide, allowing us to map the binding residue back to IGF2BP2. We first produced recombinant IGF2BP3, performed MST, and found a Kd for glucose of 7.7 μM (Fig. S4C), about the same affinity as IGF2BP2. UV-C MS found a high confidence peptide at the N-terminus of IGF2BP3 (Fig S4D-E). When performing DiffDock analysis, this peptide mapped near the binding pocket of one of the lower confidence binding modes, where two residues, Tyrosines Y5 and Y39 were both indicated as potentially interaction with glucose (Fig S4F). We produced a panel of four mutant proteins, mutating the tyrosines to alanines (Y5A, Y39A), deleting the N-terminus of the protein up until the end of the peptide nominated by UVC-MS (23a), and a deletion of the entire RRM1 domain at the N-terminus (RRM1) (Fig S4G). We found that Y5A did not shift glucose binding, but Y39A, 23a, and RRM1 variants all had ablated binding to glucose (Fig S4 H-I). In order to validate function of these mutants, we performed cross-linking immunoprecipitation (CLIP) efficiency analysis and found that IGF2BP3-Y39A maintained 79% of RNA binding (Fig. S4J-K). Residue Y39 mapped to Y40 in IGF2BP2 (Fig. S4L), and we found that IGF2BP2-Y40A had reduced binding to glucose by MST (Fig 4C). To further validate IGF2BP2-Y40A as a glucose binding mutant, we performed immunoprecipitation of recombinant IGF2BP2-WT and IGF2BP2-Y40A with glucose-biotin. We found that IGF2BP2-WT could be immunoprecipitated by glucose-biotin, and binding could be blocked with glucose competition. However, IGF2BP2-Y40A could not be precipitated with glucose-biotin (Fig 4D-E).

Glucose alters IGF2BP2 interactions with target RNAs and protein interactome

Next, we sought to study the effect of IGF2BP2 glucose binding on IGF2BP2 function in pancreatic beta cell insulin secretion. IGF2BP2 has been shown to increase insulin secretion through stabilization of PDX1, a master transcriptional regulator of the insulin production pathway (Regué et al. 2021). First, we replicated the result that knockdown of IGF2BP2 reduced insulin secretion in MIN6-6, an immortalized mouse pancreatic beta cell line with luciferase tagged insulin (Fig S4M) (Yang and Chen 2023; Burns et al. 2015). Next, we overexpressed IGF2BP2^{WT} or IGF2BP2^{Y40A} in MIN6-6 and found that IGF2BP2^{Y40A} had a dominant negative effect on cell proliferation and insulin secretion (Fig 4F-H). Because IGF2BP2 effect in insulin secretion has been shown to work through stabilization of its RNA targets like *PDX1* (Regué et al. 2021), we performed RNA immunoprecipitation and qPCR (RIP-qPCR) to quantify IGF2BP2-associated RNAs. MIN6-6 cells were starved of glucose and then treated with either 16.7 mM glucose or vehicle for 1.5 hours prior to lysis and RIP. Interestingly, we found that glucose treatment led to increased IGF2BP2 binding to known RNA targets *IGF2*, *PDX1*, and *IGF2BP2* (Fig 4I-J, note log10 scale). In order to understand the effect of glucose binding on IGF2BP2 protein-protein interactions, we performed AP-MS on HA-tagged IGF2BP2^{WT} or IGF2BP2^{Y40A} expressed in HIT-T15 pancreatic beta cells. IGF2BP2^{Y40A} showed decreased association with proteins involved in RNA-protein complex formation, ribosome biogenesis, and mitochondrial translation (Fig 4K-L), consistent with the hypothesis that glucose binding effects IGF2BP2 recruitment of client mRNAs to translational machinery (Regué et al. 2021). To further test the effect of glucose on IGF2BP2 interactome, we performed native AP-MS on endogenous IGF2BP2 purified from MIN6-6 cells starved of glucose followed by treatment with glucose or vehicle for 1.5 hours, again following the conditions used for the insulin secretion assays. Glucose treatment led to broad alterations in protein-protein interactions, including loss of interaction with Fem1b and Nkx2-2, proteins previously connected to insulin secretion and glucose homeostasis (Lu et al. 2005, Anderson et al. 2009) (Fig. 4M).

Discussion

Here we apply TPP approaches to identify new glucose binding proteins and characterize two novel glucose-binding proteins, TSC22D4 and IGF2BP2, genetically linked to metabolic disease. Glucose binding alters TSC22D4-DNA binding affinity and nuclear localization, although we were unable to confirm direct TSC22D4-chromatin interactions. Glucose binding occurs near the TSC-box, leading to increased accessibility of the C-terminal region. A space-filling I322W mutation ablates glucose binding. TSC22D4 is essential for adipocyte differentiation in the 3T3-L1 model system, and glucose binding shifts the TSC22D4 interactome away from cytoskeletal proteins and toward cytosolic and mitochondrial proteins.

IGF2BP2 binds glucose with a $K_d \approx 10$ μM, and IGF2BP2^{Y40A} showed ablated glucose binding. In pancreatic beta cells, IGF2BP2^{Y40A} overexpression had a dominant negative effect on proliferation and insulin secretion. IGF2BP2^{WT} exhibited increased association with RNA-protein complex and ribosome machinery compared to IGF2BP2^{Y40A}. Glucose increased IGF2BP2 association with client mRNAs *IGF2*, *PDX1*, and *IGF2BP2*, which are essential for beta cell maintenance and insulin secretion. Together, these results support the hypothesis that glucose binding increases IGF2BP2 binding to client mRNAs and its recruitment to translational machinery, leading to increased transcription of machinery essential for insulin secretion.

Previous work on GBPs has shown glucose rewires GBP function through altered oligomerization. However, neither TSC22D4 nor IGF2BP2 show altered oligomerization upon treatment with glucose. However, both TSC22D4 and IGF2BP2 have vastly altered protein complexing upon glucose treatment. This suggests that glucose may rewire protein interactions independent of homo-oligomerization.

One surprising result of our AP-MS studies is that both TSC22D4 and IGF2BP2 associate mitochondrial proteins in a glucose-dependent manner. Previous studies have shown that glucose re-localizes DDX21 from nucleolus to nucleus, and we also show glucose-dependent TSC22D4 nuclear localization. Future studies may assess glucose-dependent mitochondrial localization and its impact on mitochondrial metabolism.

Similar to previous work on IRF6 (Lopez-Pajares et al. 2025), TSC22D4 binds glucose near its DNA binding domain. Interestingly, glucose decreases TSC22D4 affinity for DNA, opposite the effect of IRF6-glucose binding, suggesting that similar classes of protein-glucose interactions can have different effects on protein function.

In sum, we extend previous work on GBPs in epidermal differentiation into two phenotypic systems where glucose dysregulation is a common mechanism and pathology of disease—insulin secretion and adipogenesis. This work suggests that, in addition to nutrient sensors with well-established roles in metabolic disease (e.g., AMPK, mTOR, ChREBP), direct glucose sensors may contribute to metabolic disease. Further work is required to fully understand the mechanisms by which glucose binding alters TSC22D4 and IGF2BP2 function in adipogenesis and insulin secretion

References

Amnekar RV, Dite T, Lis P, Bell S, Brown F, Johnson C, Wilkinson S, Raggett S, Dorward M, Wightman M, Macartney T, Soares RF, Lamoliatte F, Alessi DR (2024) NRBP1 pseudokinase binds to and activates the WNK pathway in response to osmotic stress. bioRxiv 2024.12.12.628181. Anderson KR, Torres CA, Solomon K, Becker TC, Newgard CB, Wright CV, Hagman J, Sussel L (2009) Cooperative transcriptional regulation of the essential pancreatic islet gene NeuroD1 (beta2) by Nkx2.2 and neurogenin 3. J Biol Chem 284:31236–31248

Burns SM, Vetere A, Walpita D, Dančík V, Khodier C, Perez J, Clemons PA, Wagner BK, Altshuler D (2015) High-throughput luminescent reporter of insulin secretion for discovering regulators of pancreatic beta-cell function. Cell Metab 21:126–137

Chen T, Xu Z-G, Luo J, Manne RK, Wang Z, Hsu C-C, Pan B-S, Cai Z, Tsai P-J, Tsai Y-S, Chen Z-Z, Li H-Y, Lin H-K (2023) NSUN2 is a glucose sensor suppressing cGAS/STING to maintain tumorigenesis and immunotherapy resistance. Cell Metab 35:1782-1798.e8

Dai N, Zhao L, Wrighting D, Krämer D, Majithia A, Wang Y, Cracan V, Borges-Rivera D, Mootha VK, Nahrendorf M, Thorburn DR, Minichiello L, Altshuler D, Avruch J (2015) IGF2BP2/IMP2-Deficient mice resist obesity through enhanced translation of Ucp1 mRNA and Other mRNAs encoding mitochondrial proteins. Cell Metab 21:609–621

Demir S, Wolff G, Wieder A, Maida A, Bühler L, Brune M, Hautzinger O, Feuchtinger A, Poth T, Szendroedi J, Herzig S, Ekim Üstünel B (2022) TSC22D4 interacts with Akt1 to regulate glucose metabolism. Sci Adv 8:eabo5555

Diabetes Genetics Initiative of Broad Institute of Harvard and MIT, Lund University, and Novartis Institutes of BioMedical Research, Saxena R, Voight BF, Lyssenko V, Burtt NP, de Bakker PIW, Chen H, Roix JJ, Kathiresan S, Hirschhorn JN, Daly MJ, Hughes TE, Groop L, Altshuler D, Almgren P, Florez JC, Meyer J, Ardlie K, Bengtsson Boström K, Isomaa B, Lettre G, Lindblad U, Lyon HN, Melander O, Newton-Cheh C, Nilsson P, Orho-Melander M, Råstam L, Speliotes EK, Taskinen M-R, Tuomi T, Guiducci C, Berglund A, Carlson J, Gianniny L, Hackett R, Hall L, Holmkvist J, Laurila E, Sjögren M, Sterner M, Surti A, Svensson M, Svensson M, Tewhey R, Blumenstiel B, Parkin M, Defelice M, Barry R, Brodeur W, Camarata J, Chia N, Fava M, Gibbons J, Handsaker B, Healy C, Nguyen K, Gates C, Sougnez C, Gage D, Nizzari M, Gabriel SB, Chirn G-W, Ma Q, Parikh H, Richardson D, Ricke D, Purcell S (2007) Genome-wide association analysis identifies loci for type 2 diabetes and triglyceride levels. Science 316:1331–1336

Franken H, Mathieson T, Childs D, Sweetman GMA, Werner T, Tögel I, Doce C, Gade S, Bantscheff M, Drewes G, Reinhard FBM, Huber W, Savitski MM (2015) Thermal proteome profiling for unbiased identification of direct and indirect drug targets using multiplexed quantitative mass spectrometry. Nat Protoc 10:1567–1593

Gaetani M, Sabatier P, Saei AA, Beusch CM, Yang Z, Lundström SL, Zubarev RA (2019) Proteome Integral Solubility Alteration: A High-Throughput Proteomics Assay for Target Deconvolution. J Proteome Res 18:4027–4037

Hauner H, Röhrig K, Spelleken M, Liu LS, Eckel J (1998) Development of insulin-responsive glucose uptake and GLUT4 expression in differentiating human adipocyte precursor cells. Int J Obes Relat Metab Disord 22:448–453
Humphrey SJ, Yang G, Yang P, Fazakerley DJ, Stöckli J, Yang JY, James DE (2013) Dynamic adipocyte phosphoproteome reveals that Akt directly regulates mTORC2. Cell Metab 17:1009– 1020
Liu W, Wang Y, Bozi LHM, Fischer PD, Jedrychowski MP, Xiao H, Wu T, Darabedian N, He X, Mills EL, Burger N, Shin S, Reddy A, Sprenger H-G, Tran N, Winther S, Hinshaw SM, Shen J, Seo H-S, Song K, Xu AZ, Sebastian L, Zhao JJ, Dhe-Paganon S, Che J, Gygi SP, Arthanari H, Chouchani ET (2023) Lactate regulates cell cycle by remodelling the anaphase promoting complex. Nature 616:790–797
Lopez-Pajares, V. et al. Glucose modulates IRF6 transcription factor dimerization to enable epidermal differentiation. Cell Stem Cell 32, 795-810.e10 (2025).
Lu D, Ventura-Holman T, Li J, McMurray RW, Subauste JS, Maher JF (2005) Abnormal glucose homeostasis and pancreatic islet function in mice with inactivation of the Fem1b gene. Mol Cell Biol 25:6570–6577
Miao W, Porter DF, Lopez-Pajares V, Siprashvili Z, Meyers RM, Bai Y, Nguyen DT, Ko LA, Zarnegar BJ, Ferguson ID, Mills MM, Jilly-Rehak CE, Wu C-G, Yang Y-Y, Meyers JM, Hong AW, Reynolds DL, Ramanathan M, Tao S, Jiang S, Flynn RA, Wang Y, Nolan GP, Khavari PA (2023) Glucose dissociates DDX21 dimers to regulate mRNA splicing and tissue differentiation. Cell 186:80-97.e26
Miao W, Porter DF, Siprashvili Z, Ferguson ID, Ducoli L, Nguyen DT, Ko LA, Lopez-Pajares V, Srinivasan S, Hong AW, Yang Y-Y, Cao Z, Meyers RM, Meyers JM, Tao S, Wang Y, Khavari PA (2025) DDX50 cooperates with STAU1 to effect stabilization of pro-differentiation RNAs. Cell Rep 44:115174
Pepelnjak M, Velten B, Näpflin N, von Rosen T, Palmiero UC, Ko JH, Maynard HD, Arosio P, Weber- Ban E, de Souza N, Huber W, Picotti P (2024) In situ analysis of osmolyte mechanisms of proteome thermal stabilization. Nat Chem Biol
Regué L, Minichiello L, Avruch J, Dai N (2019) Liver-specific deletion of IGF2 mRNA binding protein-2/IMP2 reduces hepatic fatty acid oxidation and increases hepatic triglyceride accumulation. J Biol Chem 294:11944–11951
Scott LJ, Mohlke KL, Bonnycastle LL, Willer CJ, Li Y, Duren WL, Erdos MR, Stringham HM, Chines PS, Jackson AU, Prokunina-Olsson L, Ding C-J, Swift AJ, Narisu N, Hu T, Pruim R, Xiao R, Li X-Y, Conneely KN, Riebow NL, Sprau AG, Tong M, White PP, Hetrick KN, Barnhart MW, Bark CW, Goldstein JL, Watkins L, Xiang F, Saramies J, Buchanan TA, Watanabe RM, Valle TT, Kinnunen L, Abecasis GR, Pugh EW, Doheny KF, Bergman RN, Tuomilehto J, Collins FS, Boehnke M (2007) A genome-wide association study of type 2 diabetes in Finns detects multiple susceptibility variants. Science 316:1341–1345
Van Vranken JG, Li J, Mintseris J, Wei T-Y, Sniezek CM, Gadzuk-Shea M, Gygi SP, Schweppe DK (2024) Large-scale characterization of drug mechanism of action using proteome-wide thermal shift assays. eLife
Xiao Y-X, Lee SY, Aguilera-Uribe M, Samson R, Au A, Khanna Y, Liu Z, Cheng R, Aulakh K, Wei J, Farias AG, Reilly T, Birkadze S, Habsid A, Brown KR, Chan K, Mero P, Huang JQ, Billmann M, Rahman M,

Myers C, Andrews BJ, Youn J-Y, Yip CM, Rotin D, Derry WB, Forman-Kay JD, Moses AM, Pritišanac I, Gingras A-C, Moffat J (2024) The TSC22D, WNK, and NRBP gene families exhibit functional buffering and evolved with Metazoa for cell volume regulation. Cell Rep 43:114417 Yang L, Chen W (2023) Insulin secretion assays in an engineered MIN6 cell line. MethodsX 10:102029
Zeggini E, Scott LJ, Saxena R, Voight BF, Marchini JL, Hu T, de Bakker PIW, Abecasis GR, Almgren P, Andersen G, Ardlie K, Boström KB, Bergman RN, Bonnycastle LL, Borch-Johnsen K, Burtt NP, Chen H, Chines PS, Daly MJ, Deodhar P, Ding C-J, Doney ASF, Duren WL, Elliott KS, Erdos MR, Frayling TM, Freathy RM, Gianniny L, Grallert H, Grarup N, Groves CJ, Guiducci C, Hansen T, Herder C, Hitman GA, Hughes TE, Isomaa B, Jackson AU, Jørgensen T, Kong A, Kubalanza K, Kuruvilla FG, Kuusisto J, Langenberg C, Lango H, Lauritzen T, Li Y, Lindgren CM, Lyssenko V, Marvelle AF, Meisinger C, Midthjell K, Mohlke KL, Morken MA, Morris AD, Narisu N, Nilsson P, Owen KR, Palmer CNA, Payne F, Perry JRB, Pettersen E, Platou C, Prokopenko I, Qi L, Qin L, Rayner NW, Rees M, Roix JJ, Sandbaek A, Shields B, Sjögren M, Steinthorsdottir V, Stringham HM, Swift AJ, Thorleifsson G, Thorsteinsdottir U, Timpson NJ, Tuomi T, Tuomilehto J, Walker M, Watanabe RM, Weedon MN, Willer CJ, Wellcome Trust Case Control Consortium, Illig T, Hveem K, Hu FB, Laakso M, Stefansson K, Pedersen O, Wareham NJ, Barroso I, Hattersley AT, Collins FS, Groop L, McCarthy MI, Boehnke M, Altshuler D (2008) Meta-analysis of genome-wide association data and large-scale replication identifies additional susceptibility loci for type 2 diabetes. Nat Genet 40:638–645

Fig 1. Thermal profiling proteomics identifies hexose binding proteins at physiologic concentrations

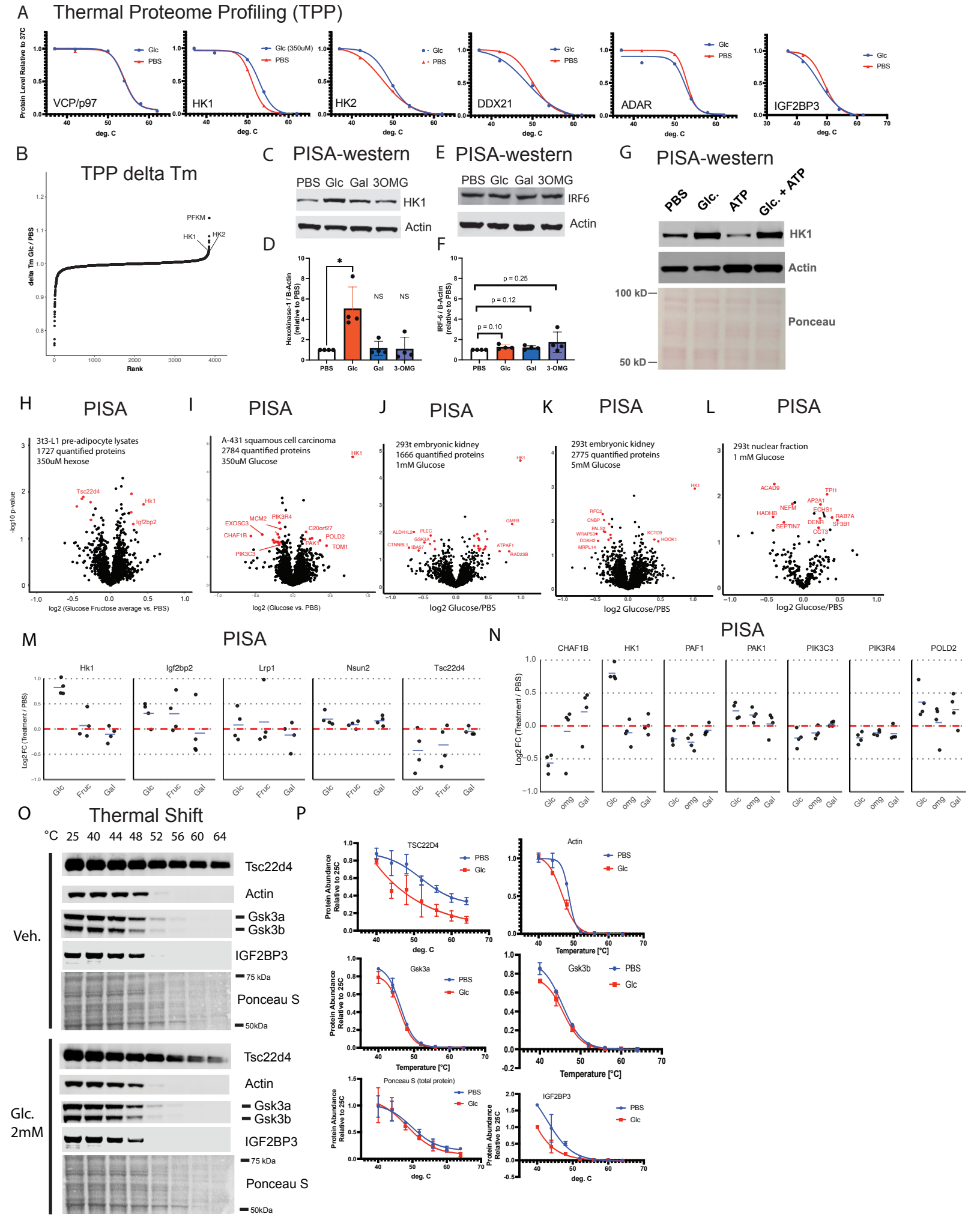

Figure 2 -TSC22D4 binds glucose at a region around I322

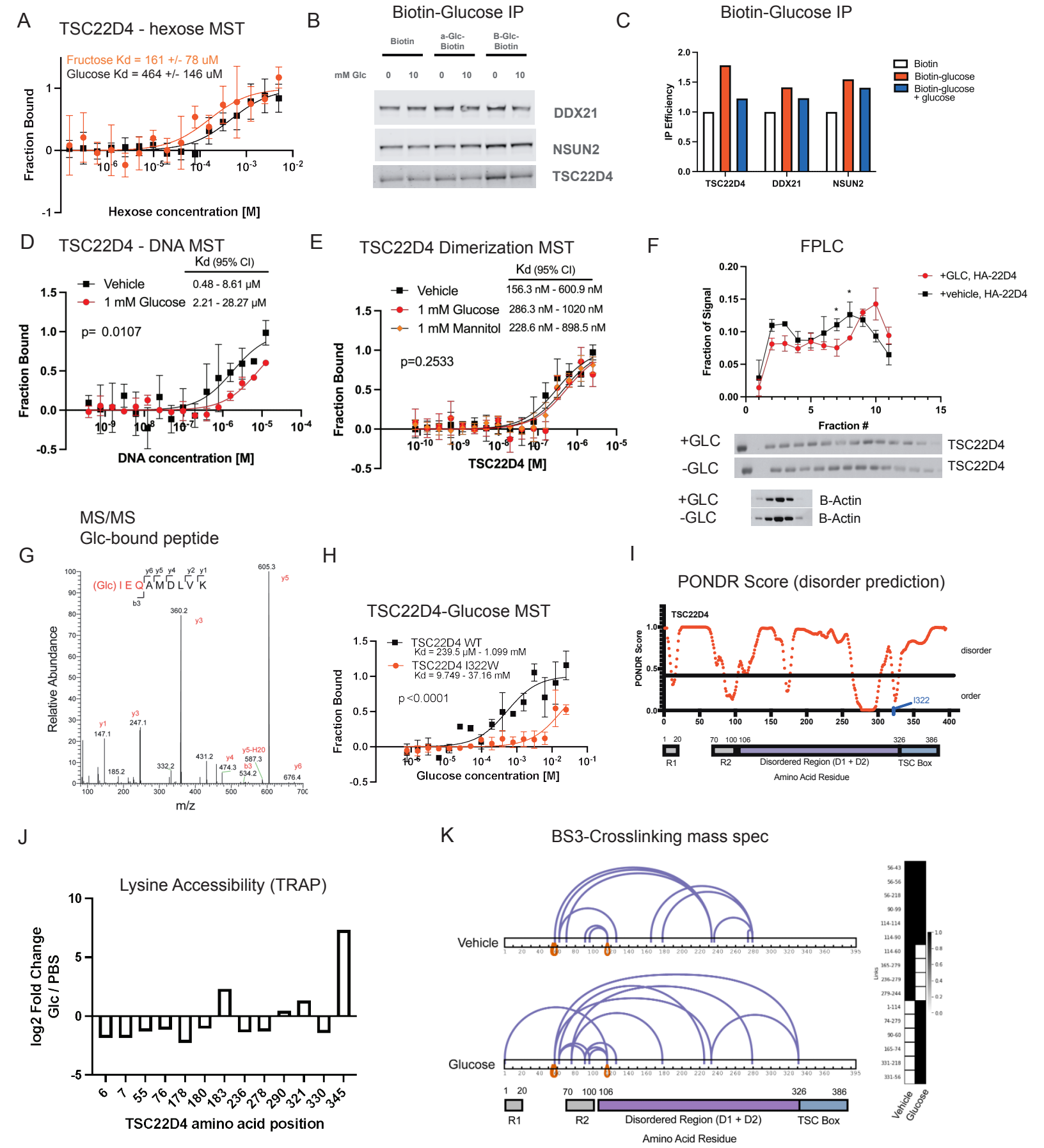

Figure 3 - TSC22D4 is essential for adipogenesis

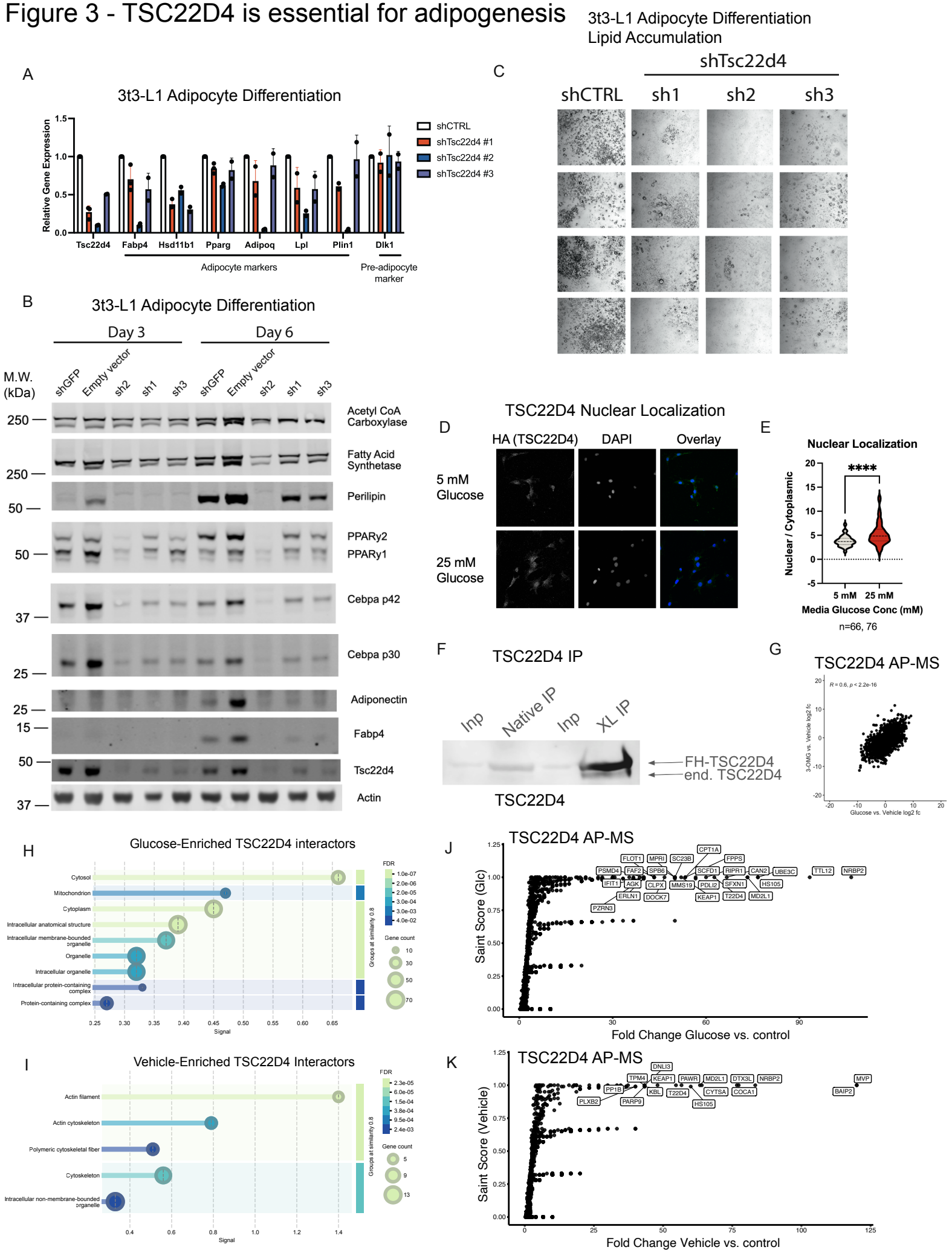

Figure 4. Glucose binding alters IGF2BP2 binding to target RNAs and protein interactome

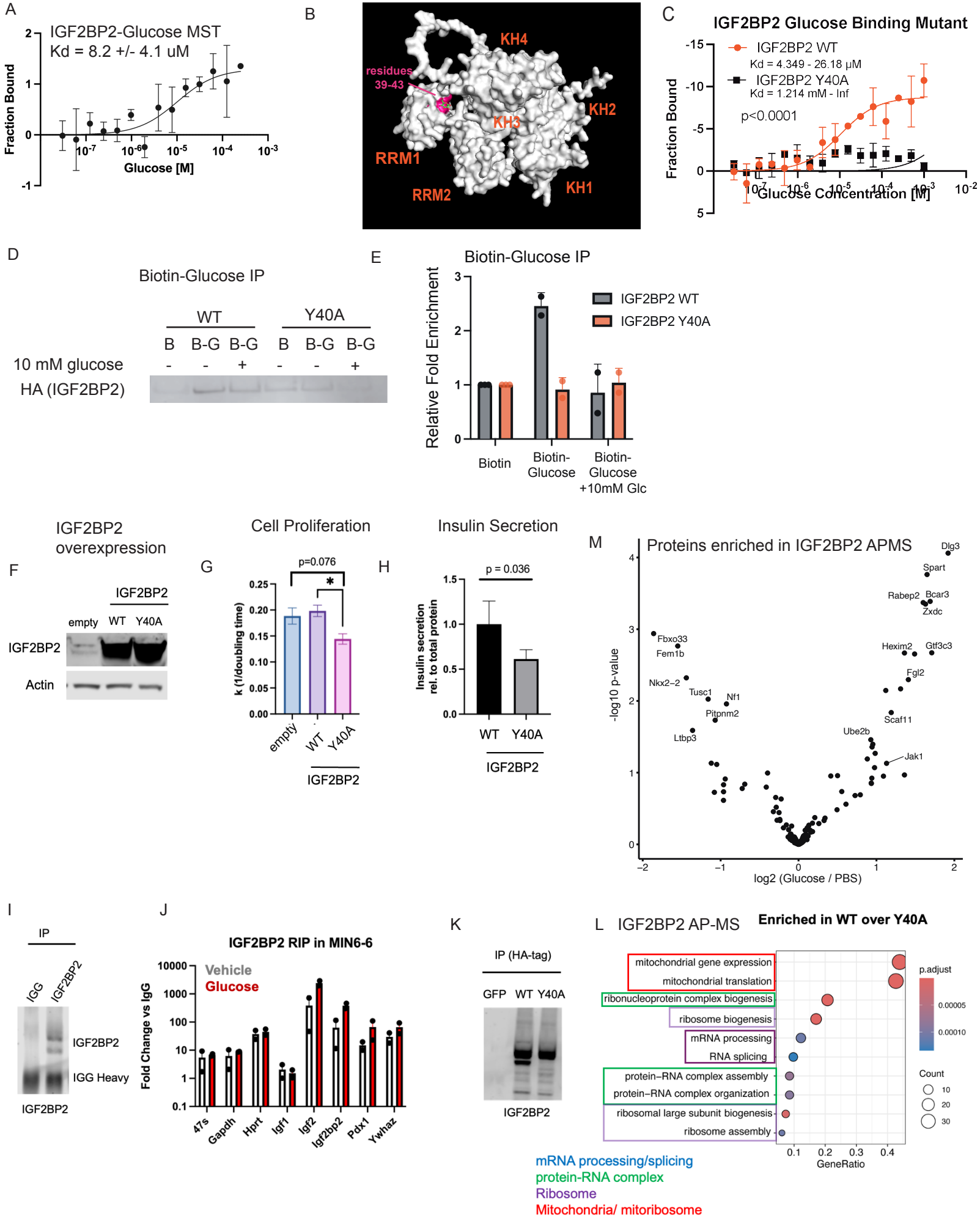

Fig S1. Thermal profiling proteomics identifies hexose binding proteins at physiologic concentrations

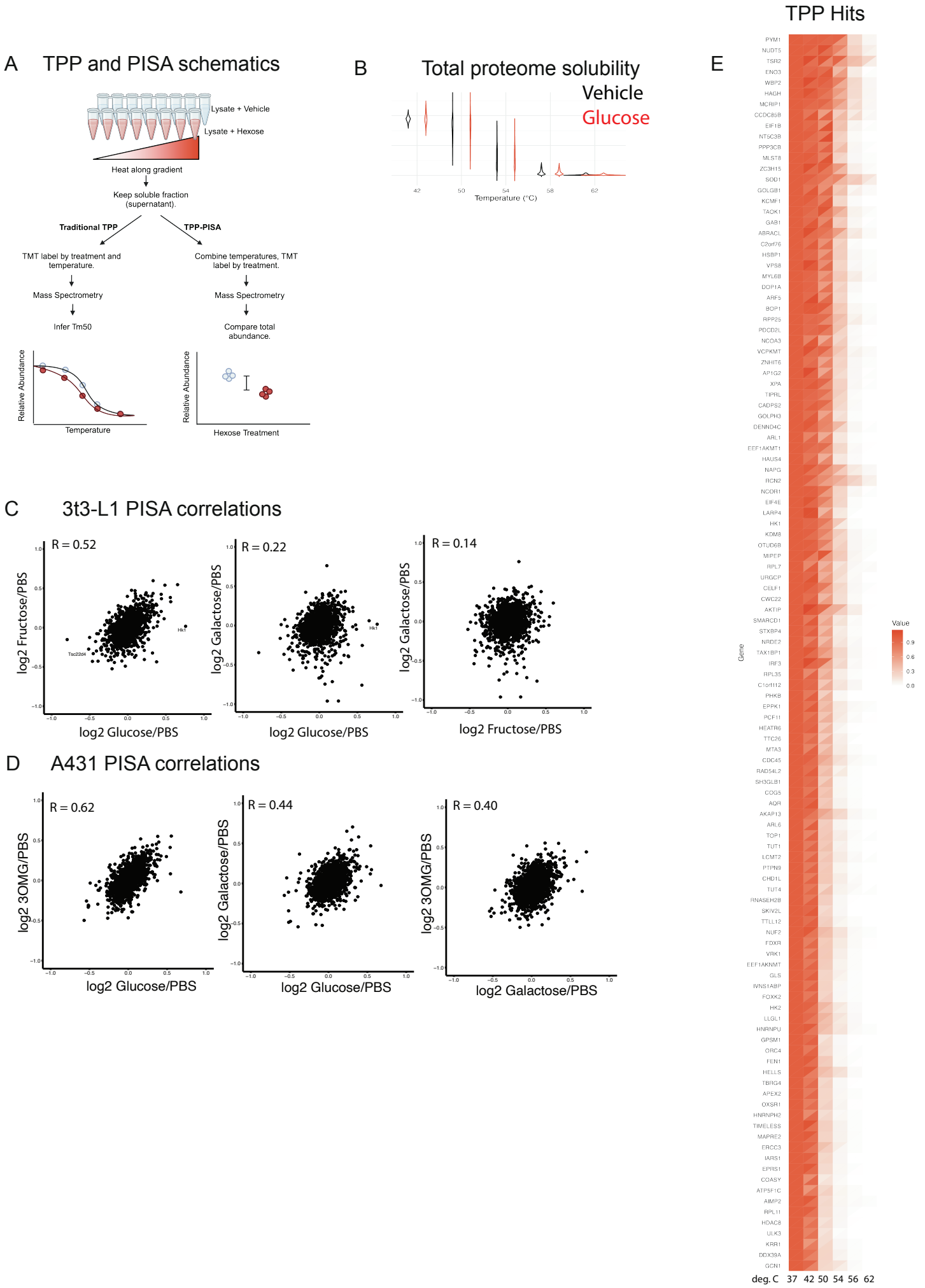

Figure S2 -TSC22D4 binds glucose at a region around I322

A

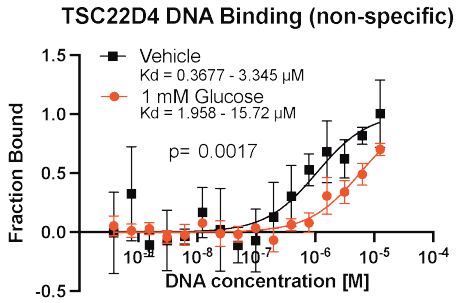

B

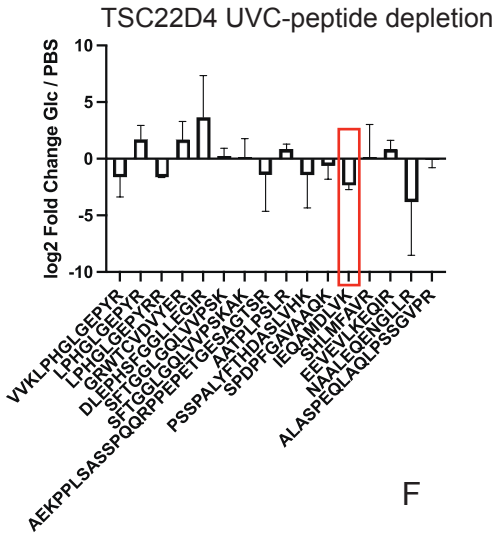

C

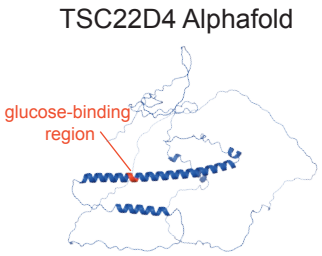

D

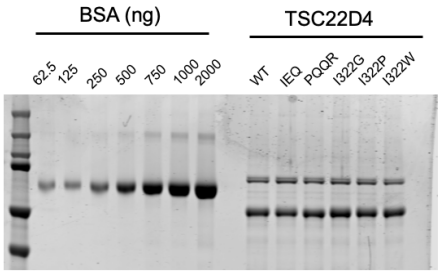

E

TSC22D4	Glucose Kd Range (95% CI) [uM]
WT	239.5 - 1099
I322W	9749 - 3716
IEQ	143.4 – 412.0
PQQR	134.9 – 405.7
I322P	411.7 – 729.1

F

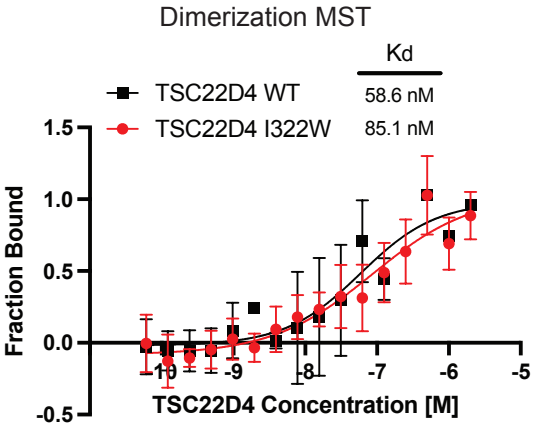

G

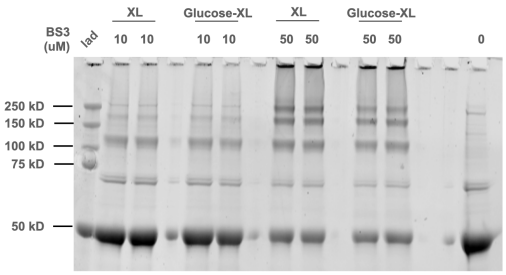

Figure S3 - TSC22D4 is essential for adipogenesis

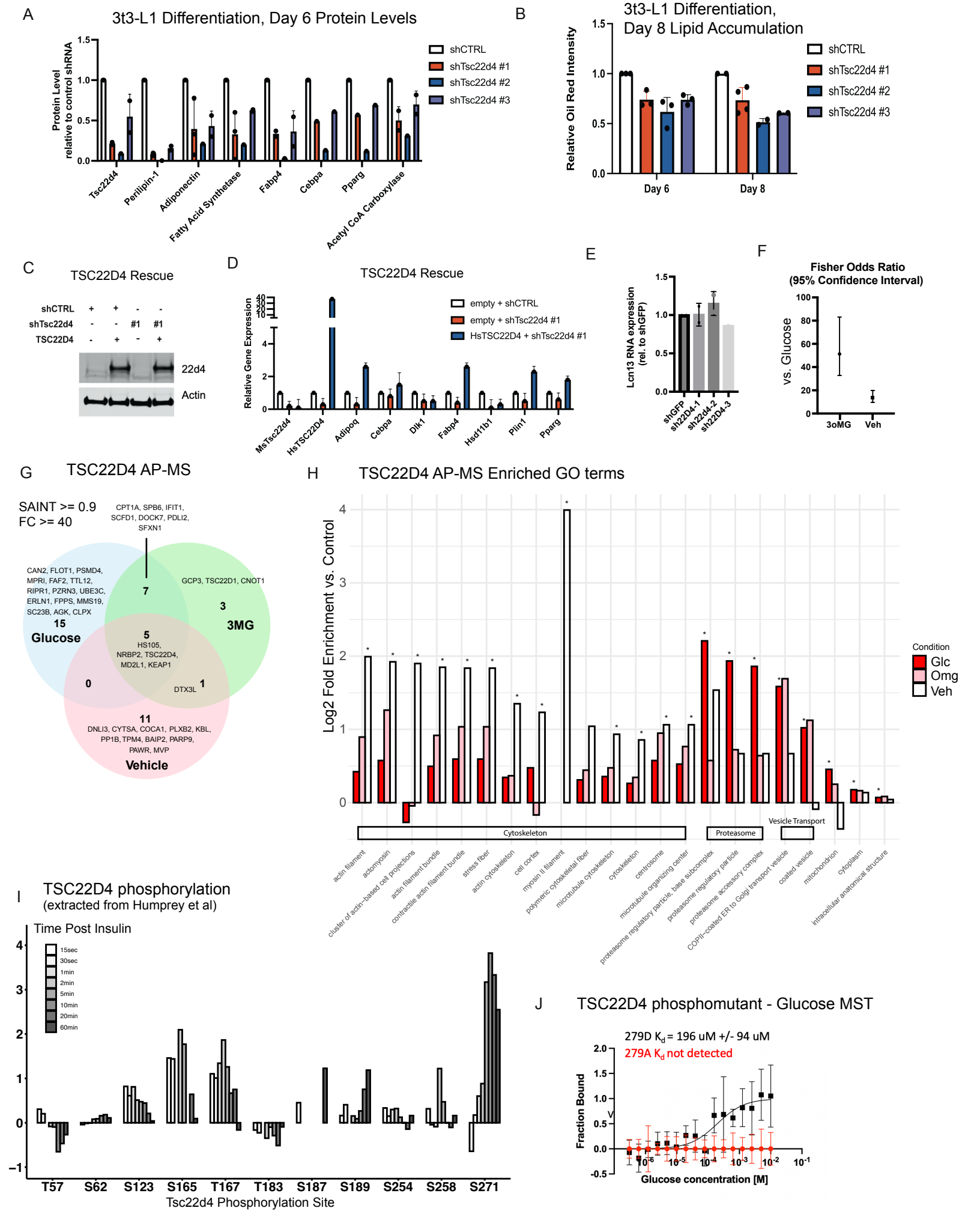

Figure S4 - Glucose binding alters IGF2BP2 binding to target RNAs and protein interactome

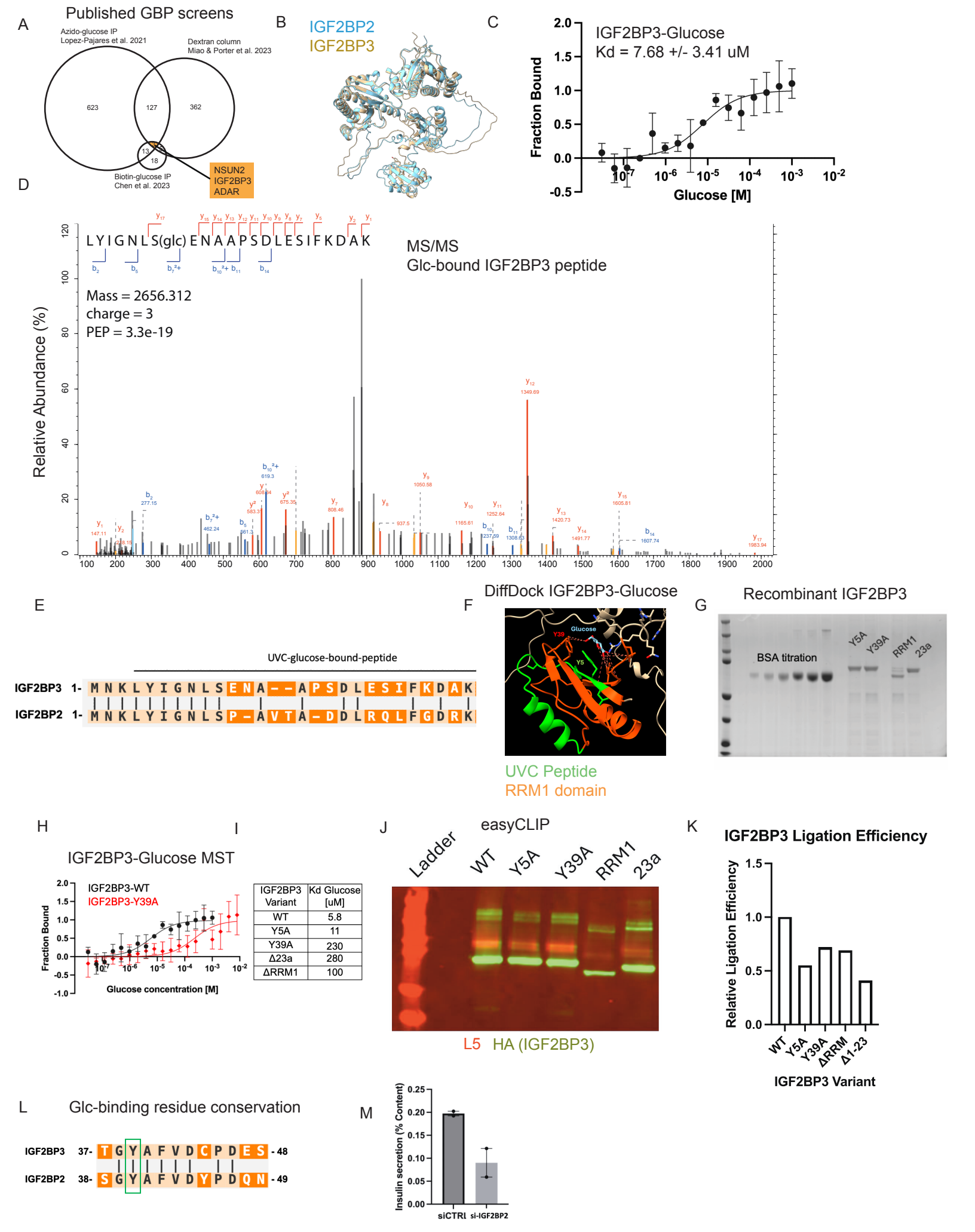

Figure 1. Thermal profiling proteomics identifies hexose binding proteins at physiologic concentrations. A) Thermal gradient profiles of proteins from Thermal Proteome Profiling (TPP) experiment. B) Rank plot of all proteins identified in experiment, showing that HK1 and HK2 are among most stabilized proteins. C-F) Western blots showing stabilization of HK1 and slight stabilization of IRF6 with glucose incubation, quantification in D and F). G) Test of 5mM Glucose and 10mM ATP for effect solubilization effect on total proteome, HK1, and Actin. H-L) Proteome in solution assays (PISA) performed in lysates extracted from 3t3-L1 pre-adipocytes (H), A431 SCC (I), and 293t (J-K, nuclear fraction in L). M-N) Log_2 fold changes for hexose treatments for individual proteins from PISA shown in (H-I). O) Thermal shift assay western profile for lysates treated with 2mM glucose or vehicle looking at targets from PISA experiments with controls. TSC22D4 and IGF2BP3 show decrease in thermal solubility under glucose treatment. P) Quantification of results in (O).

Figure 2. TSC22D4 binds glucose at a region around I322. A) MST analysis of TSC22D4 shows affinity for fructose and glucose of 161 and 464 uM respectively. B) Biotin-glucose immunoprecipitation for TSC22D4 and known glucose binders DDX21 and NSUN2. C) Quantification of results in (B). D) MST analysis of TSC22D4 and DNA oligo obtained from TSC22D4 motif in Encode dataset showing decreased binding with 1mM Glucose. E) MST dimerization analysis using labeled His-TSC22D4 and un-labeled TSC22D4 showing that neither glucose nor mannitol significantly impacts TSC22D4 dimerization. F) FPLC-western for 293t lysates treated with glucose or vehicle shows TSC22D4 distribution shift to smaller protein complexes (later elution). G) MS/MS for UVC bound peptide IEQAMDLVK. H) MST analysis for TSC22D4-I322W showing decreased binding to glucose. I) Location of I322 in TSC22D4 protein sequence. Domains are annotated based on domains proposed in Demir et al 2022 and mapped to human sequence. PONDR prediction of intrinsically disordered regions puts I322W in an ordered region above the TSC-box and to the C-terminal end of a large intrinsically disordered region (D1+D2). J) Lysine accessibility chemoproteomics showing increased labeling of lysine 345 at the C-terminus of TSC22D4. K) Intra-protein BS3 crosslinking showing induced contacts between C-terminus and N-terminus under glucose treatment.

Figure 3 – TSC22D4 is essential for adipogenesis. A) shRNA knockdown of TSC22D4 in 3t3-L1 adipogenesis with qPCR readout for differentiation associated transcript abundance. B) Western blots for differentiation markers from day 3 and day 6 of 3t3-L1 differentiation with TSC22D4 knockdown. C) Oil Red O assay stain at day 8 of differentiation with knockdown of TSC22D4, images taken with brightfield. D) Representative immunofluorescence of HA-tagged TSC22D4 in 3t3-L1 cells treated with 5mM or 25mM glucose. E) Quantification of experiment in (D) showing significant increase in nuclear localization. F) Immunoprecipitation of FH-tagged TSC22D4 with and without BS3 cross-linking in lysate. G) log2 fold changes of TSC22D4 interactome with glucose and 3-omg treatment vs. PBS control showing Pearson correlation. H-I) Gene ontology analysis of proteins enriched (SAINT >= 0.8) in glucose (H) or vehicle (I) conditions. J-K) TSC22D4 AP-MS data in glucose (J) or vehicle (K) conditions.

Figure 4. Glucose binding alters IGF2BP2 binding to target RNAs and protein interactome. A) MST analysis for IGF2BP2 and glucose. B) CB-DOCK-2 results showing placement of glucose near Tyrosine 40 in IGF2BP2 AlphaFold model. C) MST analysis for recombinant IGF2BP2 WT or Y40A mutant protein showing ablation of glucose binding. D) Biotin-glucose immunoprecipitation of recombinant IGF2BP2 WT or Y40A protein. E) Quantification of results in (D). F) Western blot analysis showing overexpression of IGF2BP2 WT or Y40A protein in MIN6-6 cells. G) Cell-titer-blue proliferation assay in MIN6-6 cells showing decrease in proliferation rate in Y40A overexpression cells. H) Luciferase-based insulin secretion assay in MIN6-6 cells showing dominant negative effect of Y40A variant overexpression. I) IP of native IGF2BP2 from MIN6-6 cells for RIP-qPCR. J) RIP-qPCR in MIN6-6 cells starved of glucose and treated with glucose or vehicle for 1.5 hours. K) IP of exogenous GFP, IGF2BP2-WT, or IGF2BP2-Y40A from HIT-T15 cells for AP-MS. L) GO analysis of AP-MS hits enriched in IGF2BP2-WT IP vs. IGF2BP2-Y40A IP. M) AP-MS of native IGF2BP2 from MIN6-6 cells starved of glucose overnight and treated with glucose or vehicle for 1.5 hours.

Figure S1. Thermal profiling proteomics identifies hexose binding proteins at physiologic concentrations. A) Schematic of Thermal Proteome Profiling (TPP) and Proteome in solution assay (PISA) methods. B) Solubility of total proteome under glucose and vehicle (PBS) conditions in TPP experiment. C) Correlations between glucose, fructose, and galactose treatments on thermal solubility in PISA assay in 3t3-L1 pre-adipocyte lysates. D) Correlations between glucose, 3OMG, and galactose PISA assay in A431 SCC lysates. E) Proteins with alterations in thermal solubility from TPP experiment.

Figure S2 - Figure 2. TSC22D4 binds glucose at a region around I322. A) MST analysis of TSC22D4 with scramble DNA oligo showing shift in DNA binding with glucose, indication glucose effect on TSC22D4 binding is not sequence specific. B) Unmodified peptide abundance changes from UVC-MS experiment showing changes with glucose binding, looking at unmodified peptides, showing loss of unmodified IEQAMDLVK peptide (boxed in red). Glucose binding events on peptides are often seen with loss of unmodified counterparts. C) I322 peptide region shown on AlphaFold structure of TSC22D4. D) Coomassie blue SDS-page analysis of purified TSC22D4 protein variants. E) 95% confidence Kd ranges for Glucose for TSC22D4 variants tested. IEQ is mutation from IEQ to GGG. PQQR denotes mutation from PQQR to GGGG, at amino acids 191-194. F) MST analysis for dimerization of TSC22D4 WT and I322W. His-tagged variant protein was paired with non-His-tagged variant protein for MST assay. G) SDS-page showing BS3 crosslinking in TSC22D4. Monomeric band isolated for mass spec runs around 50 kDa.

Figure S3 - **TSC22D4 is essential for adipogenesis.** A) Quantification of western blot data in Fig. 3B. B) Quantification of Oil Red assay data in Fig. 3C. C) Expression of TSC22D4 protein in rescue experiment. D) qPCR results of differentiation in TSC22D4 rescue experiment. E) Lcn13 transcript levels by qPCR after TSC22D4 knockdown during differentiation. F) Fisher exact test

comparing 3MG and Vehicle conditions to glucose. G) Overlap of hits from TSC22D4 AP-MS experiment**.** Target proteins with SAINT score of at least 0.9 and fold change vs control IP of 40 were selected for overlap analysis. H) Gene ontology (GO) analysis of TSC22D4 AP-MS experiment. I) TSC22D4 phosphosites extracted from Humphrey 2013, which performed phosphoproteomics analysis of 3t3-L1 cells treated with insulin. J) MST of TSC22D4 phospho-mutants with glucose.

Figure S4. Glucose binding alters IGF2BP2 binding to target RNAs and protein interactome A) Intersection of glucose binding protein mass spec experiments showing NSUN2, IGF2BP3, and ADAR as glucose binding proteins. B) Sequence alignment of AlphaFold models of IGF2BP2 and IGF2BP3 proteins. C) IGF2BP3-Glucose MST analysis showing similar affinity for glucose as IGF2BP2. D) MS/MS spectrum of glucose-linked peptide at N-terminal region of IGF2BP3. E) Sequence alignment of N-terminus of IGF2BP3 and IGF2BP2 showing sequence of glucose-bound peptide sequence found in IGF2BP3 experiment. F) Docking pose from DiffDock analysis of IGF2BP3 and glucose showing UVC peptide (green) and remaining portion of RRM1 domain (orange) with Y5 and Y39 predicted to interact with glucose. G) Coomassie gel showing recombinant protein variants of IGF2BP3. H) MST analysis showing ablation of glucose binding with Y39A mutation in IGF2BP3. I) Binding affinities obtained for various IGF2BP3 variants using MST. J) CLIP-efficiency analysis of IGF2BP3 variants. K) Quantification of results from (J). L) Homology mapping showing conservation of Y39 and Y40 in IGF2BP3 and IGF2BP2 respectively. M) siRNA mediated knockdown of IGF2BP2 in MIN6-6 cells decreases insulin secretion.

Methods

Cell culture

Lenti-X™ 293T (Takara Bio #632180) and 3T3-L1 cells were grown in DMEM + 10% FBS + PenStrep. HIT-T15 were grown in RPMI + 10% FBS + PenStrep. MIN6-6 cells were grown in DMEM + 10% FBS + PenStrep + 10 mM HEPES (Thermo #15-630-080) + 55 uM 2-Mercaptoethanol (Thermo #21985023). Beta-TC-6 were grown in DMEM + 15% FBS + 1% PenStrep. Cells were regularly tested for Mycoplasma contamination.

3T3-L1 adipocyte differentiation

3T3-L1 cells were seeded into 24-well plates and grown to confluence. Two days post-confluency (day 0), media was changed to differentiation induction media (DMEM, 10% FBS, 1% PenStrep, 10µg/mL insulin, 500uM IBMX, and 1µM Dexamethasone). Two days after induction (day 2), media was changed to growth media (DMEM, 10% FBS, 1% PenStrep, 10µg/mL insulin). Media was changed every two to three days until collection. Cells were collected at d3 and d6 for qPCR or western blot analysis, or d6 and d8 for Oil Red Staining.

Western blot

Cells were lysed in ice-cold RIPA buffer supplemented with 1X Protease Inhibitor Cocktail (Sigma, P8340). Lysates were incubated on ice for 30 minutes, then clarified by centrifugation at 20,000 × g for 15 minutes at 4°C. Protein concentration was determined using a BCA assay. Equal amounts of protein were mixed with Invitrogen™ NuPAGE™ LDS Sample Buffer (4X) (Fisher NP0008) and boiled at 95°C for 5 minutes. Lysates were loaded on 4–12% Bis-Tris gels and transferred to PVDF membranes. Membranes were blocked for 30 min at room temperature in LI-COR Intercept (TBS) Blocking Buffer (Fisher NC1660553) and incubated at room temperature for 1 hour or 4°C overnight with primary antibodies. Membranes were washed in TBS-T then incubated with LI-COR IRDye-conjugated secondary antibodies diluted 1:20,000 in PBS-T for 1 hour at room temperature in the dark. Membranes were imaged using a LI-COR Odyssey imaging system, and band intensities were quantified using LI-COR Image Studio software. Primary antibodies used were as follows: TSC22D4 (ProteinTech 55017-1-AP, Sigma HPA006757), Acetyl-CoA Carboxylase (Cell Signaling #3676), Fatty Acid Synthetase (Cell Signaling #3180), Perilipin (Cell Signaling #9349), PParg (Cell Signaling #2435), Cebpa (Cell Signaling #8178), Adiponectin (Cell Signaling #2789), Fabp4 (Cell Signaling #2120), Actin (Sigma A2228), DDX21 (ProteinTech 10528-1-AP), IGF2BP3 (ProteinTech 14642-1-AP), HK1 (Abcam ab150423), IGF2BP2 (ProteinTech 11601-1-AP), HA-tag (Cell Signaling #3724).

Plasmid cloning for overexpression and knockdown constructs

TSC22D4 and IGF2BP2 were amplified from 293t or primary human keratinocyte cDNA using CloneAmp HiFi PCR Premix (Takara) for insertion into pLEX vector using Infusion assembly (Takara). For mutations, inverse PCR was used with Infusion assembly for site directed mutagenesis. Plasmid sequences were verified by full-plasmid sequencing (Plasmidsaurus). Pooled siRNAs (SMARTPool) for mouse IGF2BP2 were ordered from Horizon Discovery. For shRNA knockdowns, target sequences were cloned in pLKO.1 (Addgene # 10878). Targeting sequences for TSC22D4 knockdown experiments are pasted below:

ID	Target sequence
sh1	GCTGGCTAGTTTGGGCATAAG
sh2	CATAAGTCTCCAGACCCATTT
sh3	CAGCTCGGGAGAGGGTATTTA
shGFP	CAGCCACAACGTCTATATCATG

RNA extraction and qPCR

Cells were collected in in RLT lysis buffer (supplemented with 1% 2-Mercaptoethanol). RNA was extracted using RNeasy Plus (Qiagen). cDNA synthesis was performed using iScript cDNA Synthesis Kit (Bio-Rad). qRT-PCR was performed using SYBR Green Master Mix on LightCycler 480 II System (Roche). Gene expression was normalized using B-actin or Hprt housekeeping genes. Primers for qPCR are included in Supplementary Tables.

Oil Red Staining

Cells were washed with PBS and fixed with 4% formaldehyde in PBS for 15 minutes. 0.2% Oil Red O (Sigma O0625) in 40% isopropanol was added to cover the plate and incubated for 30 minutes at room temperature. Plates were then washed five times with distilled water. Dye was eluted with 100% isopropanol. 200 µL of eluate was moved in technical duplicates to a 96-well plate, and absorbance was measured at 510nM on a SpectraMax M5 (Molecular Devices) plate reader.

Recombinant protein production

Lenti-X 293T cells (Takara 632180) were seeded into 15-cm plates at 70% confluency. The next day, cells were transfected with 20 µg of DNA per plate and 6.6 µg PEI MAX (Polysciences). Cells were harvested 48-72 hours post transfection. Cells were lysed in Flag lysis buffer (50mM Tris-HCl pH 7.5 150mM NaCl, 1mM EDTA, 1% Triton-X, and 1X Protease Inhibitor Cocktail [Sigma, P8340]), incubated for 30 minutes on ice, then clarified by centrifugation at 20,000xg. Lysate was incubated with anti-FLAG M2 affinity gel (MilliporeSigma A2220) for 2 hours to overnight. Resin was washed twice with Flag wash buffer (50mM TrisHCl pH 7.5, 3 mM EDTA, 0.5%NP-40, 500 mM NaCl, 10% Glycerol) and once with PBS before elution in PBS with 0.5 mg/mL Flag peptide. If necessary, eluates were dialysed in PBS overnight using Slide-A-Lyzer™ MINI Dialysis Device, 7K MWCO (Thermo 69562). Optionally, purified protein was concentrated in 10K MWCO Amicon columns (Millipore UFC500396). Finally, the target protein concentration was determined by running purified protein and a BSA standard curve on a 10% Bis-Tris gel and staining using InstantBlue Coomassie Protein Stain (Abcam ab119211).

Microscale Thermophoresis (MST)

Recombinant protein was labeled at 100nM using Monolith His-Tag labeling Kit RED-tris-NTA (Nanotemper) using 1:2 dye to protein ratio. Prior to labeling, protein was quantified by BSA standard curve in SDS-PAGE, and if necessary, protein was buffer exchanged to remove any primary amine buffer components. A 16-part dilution series (2x dilutions) of the ligand was made and labeled protein was mixed 1:1 with the ligand and incubated for 5 minutes at room temperature prior to loading into Monolith NT.115 Capillaries or NT.115 Premium Capillaries.

MST was performed using a Monolith NT.115 instrument (NanoTemper) at room temperature, using 60% excitation power and medium MST power.

RIP-qPCR and RIP-MS

MIN6-6 cells or HIT-T15 pancreatic beta cells were starved in KRBH (5 mM KCl, 120mM NaCl, 15mM HEPES pH 7.5, 25 mM $NaHCO_3$, 1mM $MgCl_2$, 2mM CaCl2, 1 mg/mL BSA) for 2 hours, then treated with 16.7 mM Glucose or PBS for 1.5 hours. Cells were washed with PBS and lysed on plate with RIP lysis buffer (140 mM KCl, 1.5 mM MgCl2, 20 mM Tris-HCl pH 7.4, 0.5% NP-40, 0.5 mM DTT, 1 U/mL RNase inhibitor, protease inhibitor), lysate was cleared at 15000g for 10 min at 4C. Lysates were precleared with 20µL Protein G magnetic beads (Pierce) for 30 min at 4°C with end over end rotation. 25 µL of Protein G beads pre-coated with 1.5µg of IMP2 antibody (ProteinTech) or HA antibody (Cell Signaling) were added to the lysates and incubated for at least 2 hours at 4°C with end over end rotation. Beads were washed four times with lysis buffer prior to elution with RLT + BME. RNA was collected with RNeasy mini column for RT-qPCR and protein flow through was precipitated with acetone for western blot and mass spec analysis. qPCR was performed as described above, with half of the immunoprecipitation used as input for the cDNA synthesis. Precipitation protein was resuspended in 50µL of 6M Urea, 50mM Tris pH 8.0, 5mM DTT with shaking for 30 minutes. 10% was removed for western blot and 90% was processed for mass spec as follows. IAA was added to 15mM for 30 minutes. Stepwise digestion was performed using Trypsin/LysC, where 2 hours of Trypsin/LysC digestion was performed in the presence of 6M Urea prior to dilution sixfold using 300µL 50mM Tris pH 8.0 for overnight digestion. Peptides were de-salted using monospin C18 columns (GL Biosciences).

Biotin-Glucose immunoprecipitation

293t cells transfected with FH-TSC22D4 construct were starved of glucose overnight (DMEM 0g/L Glc + Dialyzed-FBS + P/S). Cells were washed in PBS and collected by scraping in lysis buffer (50mM Tris-HCl pH 7.5, 150mM NaCl, 1% NP-40, 0.5% Na-DoC, protease inhibitor). Lysate was centrifuged for 10 min at 15000g at 4°C and soluble fraction collected. 500µg of protein was incubated with biotin, α-D-Glc-PEG3-Biotin, or β-D-Glc-PEG3-Biotin (Sussex Research) with or without 10mM glucose competition. MagReSyn Streptavidin beads (Resyn Biosciences) were added and incubated with end over end rotation for 1 hour. Samples were washed three times with lysis buffer. Protein was eluted with 2x LDS sample buffer + BME + 10mM biotin and analyzed by western blot.

Fast-Protein Liquid Chromatography (FPLC)

FPLC was performed as previously described (Miao et al. 2023). Lenti-X 293T cells stably infected pLEX FHH-TSC22D4 were incubated with glucose-free DMEM (Thermo 11966025) supplemented with 10% FBS and 1% PenStrep overnight. Cells were collected via trypsinization and washed twice in phosphate-buffered saline (PBS). The pellet was lysed in 10 pellet volumes of nuclei lysis buffer (20 mM HEPES, pH 7.5, 300 mM KCl, 5 mM MgCl2, 0.5 mM DTT, 1X PIC) and incubated on ice for 5 minutes. Lysates were split into two samples, and glucose was added to achieve the desired final concentration. Benzonase (Sigma E1014) was then added to reach a concentration of 3-5 Units/µL, and the samples were rotated at room temperature for 30

minutes. The samples were centrifuged at maximum speed at 4°C for 10 minutes. The resulting supernatant (250 µL) was injected into a 200 uL sample loop on AKTA machine equipped with Superose 6 Increase 10/300 column (Cytiva 29-0915-96, 10/300 GL) and Fraction collector F9-C, and the specified program was initiated. A mixture of thyroglobulin, g-globulin, ovalbumin, myoglobin, and vitamin B12 was used as gel filtration standards (BioRad, #1511901).

Docking

Protein-glucose docking to inform mutational analysis was performed using three programs, Diffdock (Corso et al. 2022), CB-Dock-2 (Liu et al. 2022), or AutoDock Vina (Eberhardt et al. 2021) using default parameters. For IGF2BP2, the AlphaFold structure (AF-Q9Y6M1-F1-v4) was docked with beta-D-glucose using CB-Dock-2.

Thermal Proteome Profiling

293T cells were grown to confluency in DMEM media and then starved overnight in 0g/L Glc DMEM+D-FBS. Cells collected by trypsinization (with quenching by 0g/L DMEM). Cells were washed 3x with ice-cold D-PBS. Pellet lysed in PISA-Lysis buffer (50 mM Tris-HCl pH 7.5, 150 mM NaCl, 1.5 mM MgCl2, 0.5% NP-40) + PIC (Sigma), incubated on ice for 15 min, and cleared with 20,000g spin at 4°Cfor 15 min. Soluble fraction was split into two tubes and treated with 350uM glucose or vehicle and incubated for 30 minutes at room temperature. Samples were split into 7 tubes and heated at 37, 42, 46, 50, 54, 58, and 62 °C for three minutes then immediately placed on ice, followed by centrifugation at 100,000g for 20 min at 4c. Supernatant was removed and transferred to new tubes. Samples were processed for mass spectrometry with each temperature-treatment pair labeled as one channel in a TMT 16plex experiment.

Proteome in Solution Assay

Cells (3T3-L1 adipocyte, A431 SCC, or 293T) were grown to confluency in DMEM media and then starved overnight in 0g/L Glc DMEM+D-FBS. Cells collected by trypsinization (with quenching by 0g/L DMEM). Cells were washed 3x with ice-cold D-PBS. Pellet lysed in PISA-Lysis buffer (50 mM Tris-HCl pH 7.5, 150 mM NaCl, 1.5 mM MgCl2, 0.5% NP-40) + PIC (Sigma), incubated on ice for 15 min, and cleared with 20,000g spin at 4°C for 15 min. Supernatant was collected and protein quantified by BCA assay (Pierce). Lysate was diluted to 2.2mg/mL and split across 16 tubes and treated with hexose sugars. Samples briefly spun down in microcentrifuge and incubated at room temperature for 30 minutes without rotation or shaking, followed by separating each sample into 8 tubes for heating in PCR machine at 44, 46, 48, 50, 52, 54, 56, 58 deg. C. After heating allowed to return to RT for 5 minutes. Equal volumes of each temperature were pooled prior to centrifugation at 20,000g, 4°C for 90 min. Soluble fractions were collected and stored at -80°C for downstream MS processing in TMT-16plex experiments.

TPP and PISA Mass Spectrometry Sample Processing

15 µg of soluble protein fraction was removed after centrifugation and placed in 200µL PCR tubes. Dilution buffer (400mM HEPES pH 8.5, 2% SDS) was added to each sample (protein denaturation). TCEP was added to 5mM and incubated for 30 minutes (protein reduction). Iodoacetamide was added to 10mM and incubated at room temperature for 30 minutes

(alkylation). DTT was added to 10mM (quench) and incubated for 15 minutes. Cleanup was performed using SP3 beads (Cytiva, 1:1 E3:E7 mix) using 10 µg of beads per µg protein. 3 µL of beads at 50 µg/µL were added to each sample and mixed by pipetting. Ethanol was added to final 50% and incubated with shaking for 15 minutes. PCR tubes were placed on magnetic rack and unbound supernatant was discarded. Beads were washed three times with 80% Ethanol. Final wash supernatant was removed and beads were air dried off the magnet. 100 µL of digestion solution (50mM TEAB pH 8.0 containing 150 ng Trypsin/LysC mix (Promega V5073)) was added to each sample and incubated at 37°C overnight with shaking at 1000 rpm. After digestion, PCR tubes were placed on a magnet and the supernatant was removed. Samples were TMT-labeled (Thermo A44521) using 2:1 TMT label:protein ratio for 45 min at RT. TMT labeling reactions were quenching with hydroxylamine prior to combining 16 reactions. Samples were de-salted and fractionated using High pH Reversed-Phase Peptide Fractionation Kit (Thermo 84868) prior to speedvac and LC-MS/MS analysis.

LC-MS/MS operation

16plex-TMT samples for PISA and TPP, TRAP samples, and TSC22D4 UV-C samples were run on Oribtrap Eclipse in 180 minute gradient with parameters as follows. In MS1, scan range of 400-1600 m/z,, maximum injection time of 50 ms, AGC target of 4e5, mass tolerance 10ppm. In MS2, CID collision energy of 35%, AGC target 1e4, mass tolerance 25 ppm. For MS3, isolation window 0.7, collision energy 35%, orbitrap resolution 50K, maximum injection 200ms, AGC target 1e5. IGF2BP3-UVC samples were run in a 190 minute method on a Fusion Lumos (Thermo). For MS1, parameters were as follows: 60K Orbitrap resolution, 300-1200m/z scan range, 50ms max injection time, AGC target 4e5. For MS2, HCD with collision energy 30%, max injection time 35 ms, AGC target 1e4.

BS3 Crosslinking Mass Spectrometry

2.5 µg of recombinant TSC22D4 protein was crosslinked at 2uM protein concentration using 50 µM BS3 in the presence of 10mM glucose or vehicle (PBS) at room temperature for one hour prior to quenching with 4X LDS sample buffer (ThermoFisher NP0008). The monomeric band was cut from the gel and processed by in-gel digestion. Thermo .raw files were converted to .mgf files prior to search with XiSearch (v 1.7.6.1) and filtered by XiFDR (v. 2.1.5.2). (Mendes et al. 2019).

In-gel digestion

Protein samples were boiled with 4X LDS sample buffer (final 1X) (ThermoFisher NP0008), run in a 10% Bis-Tris gel, and stained with InstantBlue (Abcam ab119211). The protein band of interest was cut from the gel and diced into roughly 1 mm squares. InstantBlue stain was removed with overnight incubation in 50% ACN. Samples were then reduced using 20mM DTT in 50mM ammonium bicarbonate (ABC) at 37°C for one hour. Samples were alkylated using 55mM IAA in 50mM ABC, room temperature in the dark for 30 minutes. Gel slices were washed three times with 50mM ABC. Gel slices were then washed with 100% Acetonitrile and air dried. Protein was digested overnight at 37°C using 1:50 reagent:protein Trypsin/Lys-C in 50mM ABC and 0.02% Protease Max surfactant (Promega). Peptide was extracted from digest liquid, two elutions with 5% acetic acid, and two elutions with 2.5% acetic acid, 50% acetonitrile. Elutions

were pooled and any extra SDS-Page gel was removed using Spin-X 0.22uM column prior to speedvac and de-salt using MonoSpin columns (GL Sciences) and analysis by mass spec.

UV-C Mass Spectrometry

Glucose UV-C crosslinking mass spectrometry was performed as previously described (Miao et al. 2023). Briefly, recombinant protein was diluted to 200 nM and incubated with glucose (10 mM for TSC22D4, 20 uM for IGF2BP3) at room temperature for 15 minutes, aliquoted into 3 uL droplets on parafilm, and subjected to 254 nm UV-C light (UV Stratalinker 2400) at 0.3 J/cm^2. All droplets for each sample were combined, boiled in LDS, and subjected to in-gel digestion prior to LC-MS/MS analysis.

Target Response Accessibility Profiling (TRAP)

3 µg of Recombinant TSC22D4 was incubated with 10mM glucose or vehicle for 30 minutes at room temperature. Deuterium Formaldehyde (CD20) was added to a final concentration of 0.03% and Borane Pyridine Complex (BPC) was added to 3.65mM. Reaction was incubated for 30 minutes at room temperature prior to quenching with 50mM NH4CO3. Protein was processed for mass spectrometry using Filter-Aided Sample Preparation (FASP) method. Briefly, sample was filtered using 10 kDa column at 12,000g spin for 15 minutes. Protein was denatured using 8M Urea for 30 min, reduced with 5mM DTT at 56°C for 30 minutes, and alkylated with 20mM IAA for 30 min at room temperature. 10 mM DTT was added to quench IAA and protein was washed twice with NH4CO3. 60 ng trypsin per sample was added in 50mM TEAB digestion buffer. Peptides were collected from the column and desalted with monospin C18 prior to LC-MS/MS analysis.

Affinity Purification Mass Spectrometry

3T3-L1s stably expressing HA-tagged TSC22D4 were grown to 90% confluence, washed once with PBS, then treated with glucose-free DMEM (Thermo 11966025) + 10% FBS for 4 hours, incubated 1 hour with DMEM 10% FBS with 25 mM glucose or 25 mM 3-OMG, then collected by trypsinization. Cell pellets were stored at -80C. Pellets were lysed on ice for 30 minutes in 5X pellet volume with 50 mM HEPES, pH 7.5, 100 mM NaCl, 0.2 mM MgSO4, 1% Triton X-100, 1X Halt Protease/Phosphatase Inhibitor (Thermo 78440), and clarified by centrifugation (20,000xg for 10 min at 4°C). Supernatant was collected and quantified by BCA assay. BS3 (Thermo A39266) was added to a final 1 mM concentration and incubated for 30 minutes at RT. 0.4 mg of lysate was used for IP, and IP volume was made up to 1 mL with lysis buffer. 20 uL of anti-HA Dynabeads (Pierce) were added to lysate and incubated with end-over-end rotation at 4C overnight. Beads were washed three times with 500 uL of IP buffer for 5 minutes each. Proteins were eluted off beads in 30 uL 2X LDS sample buffer with 90 degC heating for 5 min. Samples were then run on SDS page and processed with in-gel digestion for mass spec.